X International Conference on Computational Methods in Marine Engineering
MARINE 2023
J. Garcia-Espinosa, L. González, J.E. Gutiérrez & B. Serván-Camas (Editors)

Computer Vision Approach for Pipeline Slug Flow Analysis

Jose D. Mesa[1*], Kyle Porter[2] and Eduardo Pereyra[3]

[1]Anaconda Inc., Austin, TX 78701, United States

[2]Department of Mechanical Engineering, The University of Tulsa, Tulsa, OK 74104, United States

[3]McDougall School of Petroleum Engineering, The University of Tulsa, Tulsa, OK 74104, United States

[*]jmesa@anaconda.com

ABSTRACT

In recent years, there has been growing interest in understanding the impact of internal, two-phase flow-induced vibration (FIV) on pipeline fatigue life, particularly in the oil and gas industry. The complex gas-liquid internal interactions can produce what is known as slug flow. Slug flow can be defined as significant periodic changes in gas or liquid volumes in pipeline sections, which introduce pressure fluctuations resulting in FIV. To this end, the University of Tulsa conducted a series of experimental tests aimed at replicating pipeline behavior under loadings from slug flow. A novel in-house image-processing technique was used to extract data on internal two-phase flow interaction and provide benchmarking data for numerical modeling. This technique utilized binary square fiducial markers to track pipe response and color segmentation to distinguish the gas-liquid interface. The resulting data, which included measurements of volume fraction, was compared with traditional conductance probe measurements to identify any discrepancies in the current experimental recording systems. The project's goal is to provide a comprehensive data set to support the evaluation of current design and analysis methodologies, as well as numerical tools.

Keywords: Computer Vision; Fluid-Structure Interaction; Machine Learning; Multiphase-Flow; Experimental Testing; Slug Loading.

NOMENCLATURE

Δy	Vertical change in marker position [m]
Δt	Change in time [s]
Δv	Change in marker velocity [m/s]
$\Delta L_{i \to j}$	Length between probes [m]
L	Slug length [m]
τ^*	Temporal lag during cross-correlation [-]
f	Frequency [Hz]
n	Number of occurrences [-]

1. INTRODUCTION

Recently, the offshore oil and gas industry has begun to pay more attention to the impact of long-term fatigue caused by internal, flow-induced vibrations (FIV), particularly related to slug flow. As the life of offshore assets progresses, the gas-to-liquid ratio flowing in production risers typically increases, leading to more frequent slugging events. A slug event can be defined as a significant periodic change in gas or liquid volumes in pipeline sections, introducing pressure fluctuations that result in substantial pipe vibrations. The change in gas-to-liquid production ratio, combined with complex geometries such as lazy wave risers or scarp-crossing pipelines, has raised concerns about slugging-induced fatigue consuming excessive fatigue capacity in production systems. In fact, for several lazy wave risers and pipelines with scar-crossing sections in shallow water, slugging-induced fatigue has already been identified as a governing design case for the flowline integrity (Mesa et al., 2022). However, modeling the fluid-structure interaction (FSI) in these systems is challenging due to the complex two-phase fluid behavior and dynamic structural response (Porter et al., 2022). Even state-of-the-art methodologies for numerically investigating FIV in pipes require benchmarking against the results of experimental studies to ensure their validity (Miwa et al., 2015).

This paper focuses on a computer vision technique that supports extracting experimental data for validating numerical modeling. While traditional recording systems provide excellent discrete data sources, they fall short of coupling the entire test section interaction and correlating the flow parameters with the structural response. In this paper, we study slug characterization using an in-house computer vision methodology that supports evaluating the relationship between flow parameters and structural response through experimental testing.

2. EXPERIMENTAL CAMPAIGN

The experimental campaign presented in this study was performed at the Tulsa University Fluid Flow Projects (TUFFP), a low-pressure flow loop with a 6-inch internal diameter (Porter et al., 2022). The experimental facility consists of two separate delivery systems for fluid phases, air (gas phase) and water (liquid phase). The flow loop starts with a roughly 37-meter horizontal developing section after the mixing inlet, followed by a 1-meter corrugated hose. The roughly 10-meter of flexible test section follows and is also horizontal. A corrugated, U-shaped hose is attached to the test section outlet to divert the fluid into the return line and help absorb system vibrations safely. The corrugated hoses before and after the test section also serve to decouple the flexible test section motion from the rest of the system.

The test section, as shown in Figure 1, is made of flexible, transparent polycarbonate material. The material's flexibility magnifies deflections and vibrations during experimentation, making differences in structural response more distinguishable. The pipe's transparency enables non-intrusive measurement of the liquid distribution inside. The test section boundary conditions are simply-supported to simulate typical offshore pipelines (Mesa et al., 2022) and model the more conservative results in terms of vibration and fatigue (Kansao et al., 2008). The test section is designed to simulate the behavior of a horizontal pipe. However, the weight of the pipe can cause it to sag, which in turn can cause flow stratification and make it difficult to obtain accurate flow data. To overcome this issue, a spring support has been installed at the center of the test section. The spring support allows for deflection due to soil stiffness while preventing self-weight deflection. This simplifies the internal flow interaction, making it easier to obtain accurate data without the need for complex scaling adjustments. The spring support design also provides a more realistic coupling of flow characteristics and vibrational relationship, resulting in a more accurate simulation of real-world conditions.

To enhance the accuracy and reliability of the computer vision results and the data collected by the cameras, a blue backdrop has been constructed behind the test section. The blue color provides a strong contrast to the white and black markers used to track the pipe motion, as well as the yellow/green fluorescent dye added to the water. In addition, an awning has been constructed over the entire test section to ensure that changes in lighting do not significantly affect the accuracy of the computer vision data.

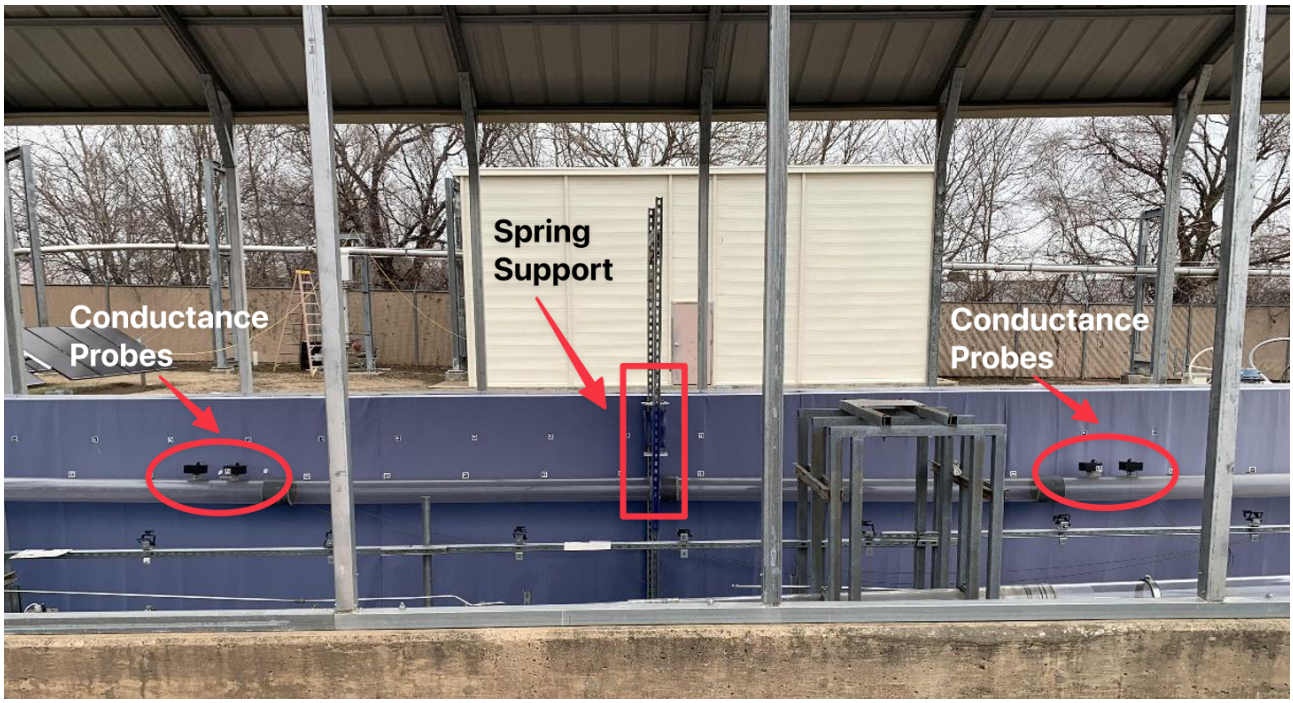

Figure 1 - Experimental 10-meter flexible, polycarbonate, 6-inch ID, pipe test section.

3. COMPUTER VISION METHOD

As mentioned, previous experimental campaigns depend on commonly used instrumentation such as accelerometers, load cells, or strain gauges to measure the pipe response. The main disadvantage of these measurement systems is that they are discrete and can only provide information at specific locations decoupling the system response. Furthermore, the correlation between the internal two-phase flow and the system response had to be done separately, which can introduce other challenges. In this study, we deploy an image processing technique that detects a particular binary square fiducial marker type allowing for continuous system response tracking and simultaneous correlation of the internal flow with the overall system response.

The binary square fiducial marker deployed in this study is the ArUco marker. ArUco markers were deployed at the top of the pipe (tracking purposes), and blue backdrop (reference datum). Augmented Reality University of Cordoba (ArUco) markers were developed specifically for detection in images and videos (Garrido-Jurado et al., 2014). An example of an ArUco marker installed on the test section is shown in Figure 2, which greatly resemble the standard QR codes encountered daily.

The ArUco marker's inner binary codification allows them to display robust detection within images or videos, even when angled or partially obscured. This creates a significant improvement in the consistency of pipe tracking compared to the image processing techniques used in previous studies. For example, (Mesa et al., 2022) tracked pipe motion using color segmentation to identify red markers affixed to the pipe. The contrast of the red color to the background of the video allows the authors to identify the location of the centroid of the square in each video frame. However, not only did the region of interest (ROI) for tracking the markers require manual initialization for each video, but there was much inconsistency in the color contrast, and therefore the marker identification.

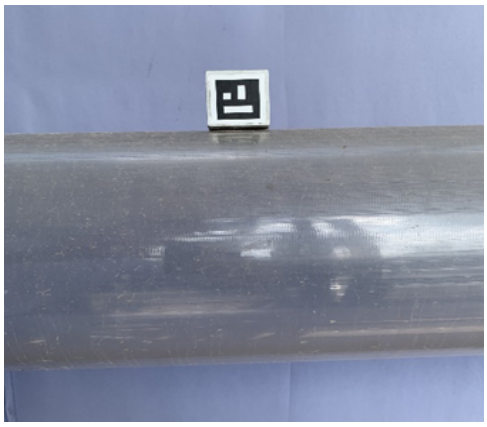

Figure 2 - ArUco marker example from the test section.

In this study, we installed 26 ArUco markers along the top of the test section, spaced approximately every 0.5 meters. Another set of 26 markers was installed on a blue backdrop directly above the pipe markers. The large number of pipe markers allows for linearizing the non-linear pipe curvature during deflection. The backdrop markers serve as reference line markers, which have two functions: providing a reference datum for measuring deflection and a straight line that is captured in the video data and used to correct camera rotation. We developed an algorithm using a combination of in-house programming and open-source packages. The OpenCV (Bradski, 2000) Python library was used to manipulate the video frames and detect markers. The algorithm searches each frame for marker detection by identifying their unique black-and-white pixel sequences. An example of a frame before and after detection is shown in Figure 3.

The corner locations of the ArUco markers are used to determine the centroid of the marker, which is then expressed as an x-y pixel location. For this study, only y-pixel displacement is significant since the pipe deflections are mainly in the y-direction and boundary conditions restricted axial displacement. The x and y pixel locations of the centroid are stored in a Python dictionary until all frames for a given video have been analyzed. The data is then converted to a data frame, where consistency checks are performed on the marker detection. Although markers are typically detected in all frames, data may be linearly interpolated to ensure continuity in case of temporary obscuration. Knowing the pixel displacement and the size of the markers allows for conversion to actual displacement in units of length. The actual pipe deflection is determined by subtracting the displacement from the reference datum of the pipe markers during an empty test (no gas or liquid flowing).

The range of markers positioned to be captured by each individual camera is intentionally selected so that each camera along the test section has at least one shared pipe marker with the subsequent camera. The deflection of the markers creates a time series signal for each camera, which should be identical for the shared markers. However, the delays in the start time of each camera cause the signals for the shared markers to become out of sync. To solve this issue, the delays in the start time of each camera are analyzed using a cross-correlation algorithm that detects the delay (in terms of the sampling frequency) between each camera by analyzing the signals. The time series deflection data is corrected accordingly so that all the extracted videos are time-synchronous within one frame. The result is an accurate time series of the deflection for each marker on the pipe. To visualize how the pipe deflection data is digitized and synchronized, a complete digital reconstruction of the test section is shown in Figure 4. Each point in the figure represents a pipe marker, and the colors distinguish which camera the data came from. The digital reconstructions can be used to validate that marker data was captured and synchronized correctly and could allow for future numerical finite element method (FEM) simulation and theoretical solution validations.

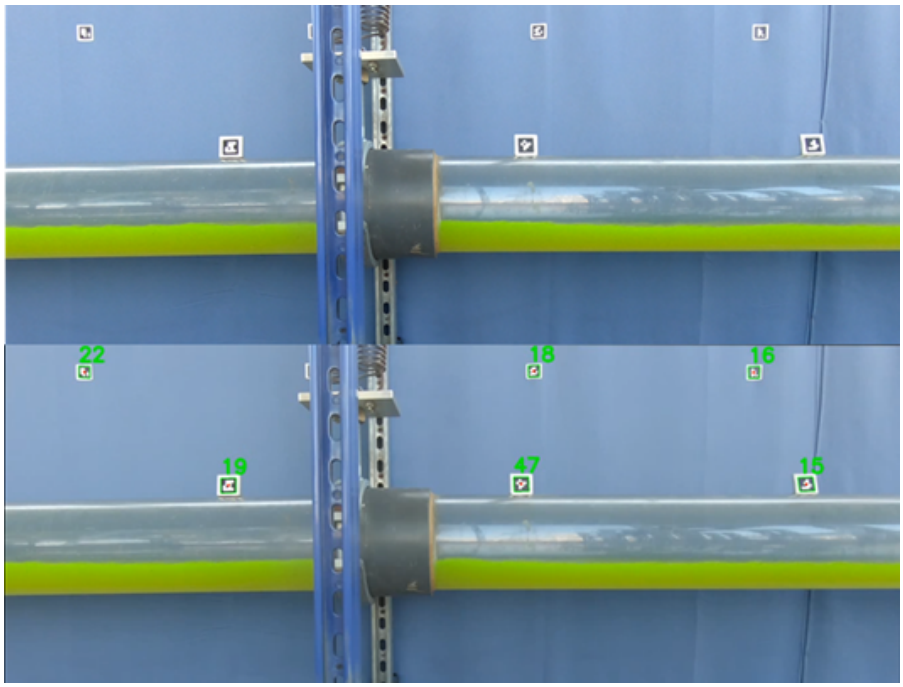

Figure 3 - Original frame from the video (top) and frame after performing marker detection (bottom).

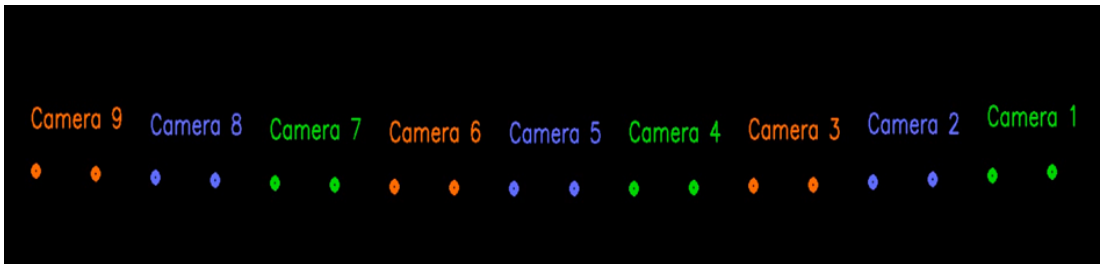

Figure 4 - Digital reconstruction of pipe motion via marker data (not to scale).

The in-house algorithm calculates the velocity (m/s) and acceleration (m/s^2) from the data using Equations (1) and (2), respectively.

$$v = \frac{\Delta y}{\Delta t} \tag{1}$$

$$a = \frac{\Delta v}{\Delta t} \tag{2}$$

Where Δy is the vertical change in marker position (m), and Δt is the change in time (s).

Computer vision techniques were used to extract fluid parameters as well, which had been done in only a handful of previous studies and in a limited capacity. For example, Ahmed (2011) investigated the internal flow characteristics by designating each pixel value in every video frame as either zero or one based on its gray level, effectively binarizing the image into locations of gas or liquid based on pixel contrast. Mohmmed et al. (2016) also employed this thresholding process to binarize images and used foreground and blob extraction to identify a region of interest (ROI) for motion tracking. The foreground and blob identified passing slugs as the ROI and tracked the ROI location in each subsequent frame, enabling the calculation of slug characteristics such as translational velocity and length by utilizing the known framerate.

In this study, color segmentation is the primary image processing technique utilized to identify gas and liquid locations within a video frame. Unlike the binarization method used by other authors, color segmentation identifies areas of an image based on their color or hue. This technique was chosen for its ability to accurately identify gas and liquid locations, even in complex flow regimes. Initially, the location of the pipe is detected using the ArUco markers, as shown in the previous section. Accurate detection of the markers is crucial to ensure that the algorithm can adjust its ROI for liquid detection in each frame, as the test section constantly changes location. Once the marker locations are known, a smaller image containing the pipe section between each set of markers is cropped from the larger image, such as in Figure 5, which shows a cropped image of the pipe section between two markers.

Figure 5 - Example of a cropped image from the pipe section between markers.

For each pixel in Figure 5, the computer contains data on hue, saturation, and value (HSV). This metadata in the image tells the computer what color to display at a given pixel in the image array. The cropped image can be "color segmented" by applying a "mask" to the array of pixel color values. Again, a combination of in-house programming and OpenCV (Bradski, 2000) is used to read, manipulate, and alter the frames from the video. In color segmentation, a mask is a filter that is applied to an image to extract specific colors or color ranges. By applying a mask to filter the yellow/green color, an array of ones and zeros denoting liquid and gas is created. This process is called binarizing the image, and the result is shown in Figure 6. The blue color is used for a background because it is on the opposite end of the hue spectrum from the yellow/green color of the liquid, which provides a more accurate binarization of the image by clearly separating the liquid and gas regions.

Figure 6 - The cropped image in Figure 5 after being binarized.

The slug characteristics can be extracted using the liquid holdup signal from two points (“virtual probes”) along the test section. We created 17 virtual liquid-level probes, each roughly 0.3 meters apart and centered between each set of ArUco markers and used a threshold value of 0.9 to distinguish between slugs and liquid film. We filtered the binarized signal to exclude small waves or bubbles within a continuous slug/film unit to accurately capture slug lengths and frequencies. Figure 7 shows an example of signal processing using the video feed, where the red lines represent the liquid-gas interface detected by the algorithm, and the black rectangles show the locations of the virtual liquid-level probes. The algorithm also displayed the word "SLUG" on the output video along with the interface line and probe rectangles for manual verification.

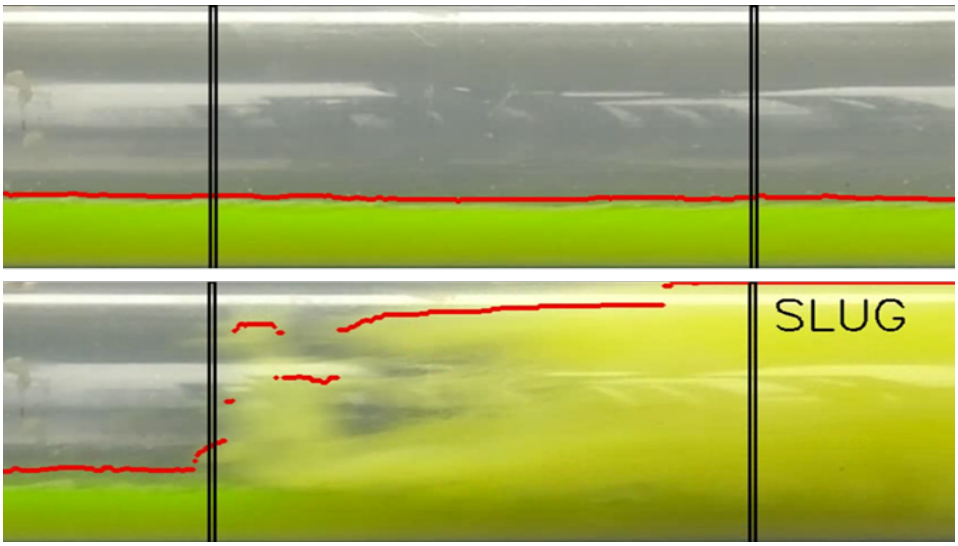

Figure 7 - Film (top) and slug (bottom) detection from video data.

From these signals, slug translational velocity, length, frequency, and average film holdup can be calculated. Slug translational velocity (m/s) is calculated using a cross-correlation algorithm to determine the lag between the signals of two adjacent probes with a know distance. Slug translational velocity is calculated using Equation (3).

$$v_t = \frac{\Delta L_{i \to j}}{\tau^*} \tag{3}$$

Where $\Delta L_{i \to j}$ is the distance between two adjacent probes (m), and τ^* is the temporal lag calculated via cross-correlation. The slug length (m) can then be calculated by knowing the time interval for the slug to pass the probe, as shown in Equation (4).

$$L_s = v_t \Delta_{ts} \tag{4}$$

Where Δ_{ts} is the time interval the slug is at the probe (s). Finally, the slug frequency (Hz) can be calculated in Equation (5) by counting the number of slugs identified in the signal processing.

$$f_s = \frac{n}{t} \tag{5}$$

Where n is the total number of slugs that pass the probe during the test and t is the total test duration (s). It is important to note that the methodology applied in this study does have the capability to distinguish between slugs and pseudo-slugs.

4. SYSTEM RESPONSE EXTRACTION VIA COMPUTER VISION

In this section, we use computer vision methodology to extract data on the pipe response and internal slug characteristics. Table 1 shows the experimental test matrix discussed in this paper. To facilitate data analysis and assess the benefits and limitations of the computer vision method, we maintained a constant liquid superficial velocity of 0.3 m/s while varying the superficial gas velocity from 2.0-15.0 m/s.

Test Case	V_{SG} (m/s)	V_{SL} (m/s)
Case 1	2.0	0.3
Case 2	4.0	0.3
Case 3	15.0	0.3

Table 1 - Experimental test matrix conditions.

To ensure the accuracy of our in-house computer vision methodology, we conducted benchmarking of liquid holdup (volume fraction) using conductance probes, as shown in Figure 8. Although these two signals are not perfectly synchronized and were manually aligned based on the test case start time and slug passages for comparison purposes, both methodologies demonstrate good agreement, with discrepancies observed in the maximum predicted liquid holdup magnitude. The computer vision method's inability to account for gas entrainment compared to the conductance probe results in an overestimation of the liquid holdup magnitude, as seen in Figure 8. As more gas is added, the difference in liquid holdup from the two sources increases, as cameras cannot capture the increase in slug aeration.

Despite tending to over-predict the liquid holdup magnitude, the computer vision methodology is a more scalable and robust method than the conductance probes. The signal processing utilized to identify slug or film regions is based on a threshold value. The computer vision methodology has the distinct advantage of utilizing a consistent value for thresholding. Additionally, the verification of accurate processing can easily be validated by observing the video data. In contrast, the threshold value for signal processing using conductance probes must be constantly adapted to account for the entrained gas in the system. While there are methods that attempt to address this issue, they are challenging to implement and contain a great degree of uncertainty. These challenges in processing the signal from conductance probes are further aggravated by the uncertainty in normalizing the signal (using empty and full signal values) and due to the high degree of noise in the signal. The difference in signal noise between the methodologies can be seen clearly in Figure 8.

Figure 9 shows the time history of pipe midpoint deflection, which was extracted from camera recordings. As seen in Figure 9, the magnitude of deflection tends to decrease as the gas superficial velocity increases. The displacement time history shows that at low gas velocities, the slugs and bubbles behave more like a regular slug train. In contrast, a more complex internal interaction occurs at high gas velocities, resulting in a more erratic slug train.

As previously mentioned, one of the major advantages of the computer vision methodology is its ability to extract not only internal flow data but also overall pipe response in a synchronized manner. Figures 10, 11, and 12 demonstrate this capability by depicting instances where the method detected a slug and the corresponding pipe frequency analysis (FFT) for that flow condition. The figures show that the dominant frequency tends to increase as the gas superficial velocity increases. Moreover, the dominant system response frequency corresponds to the slug frequency, and as the gas velocity increases, more frequencies are excited. This excitation of multiple frequencies is due to the generation of several slugs with varying characteristics (e.g., length, velocity) at higher gas velocities. This effect is observable in Figures 10, 11, and 12, where lower gas velocities have one dominant frequency and less sparse excitation, whereas higher gas velocities have several dominant frequencies and a more distributed excitation range.

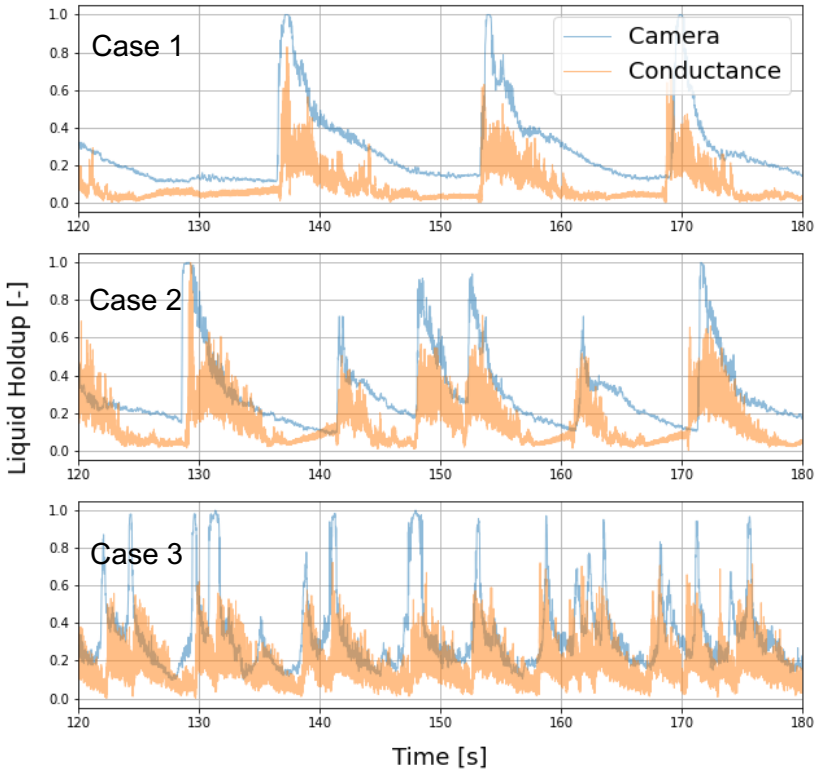

Figure 8 - Computer vision extracted data (blue line) and conductance probe (orange line) liquid holdup time series comparison.

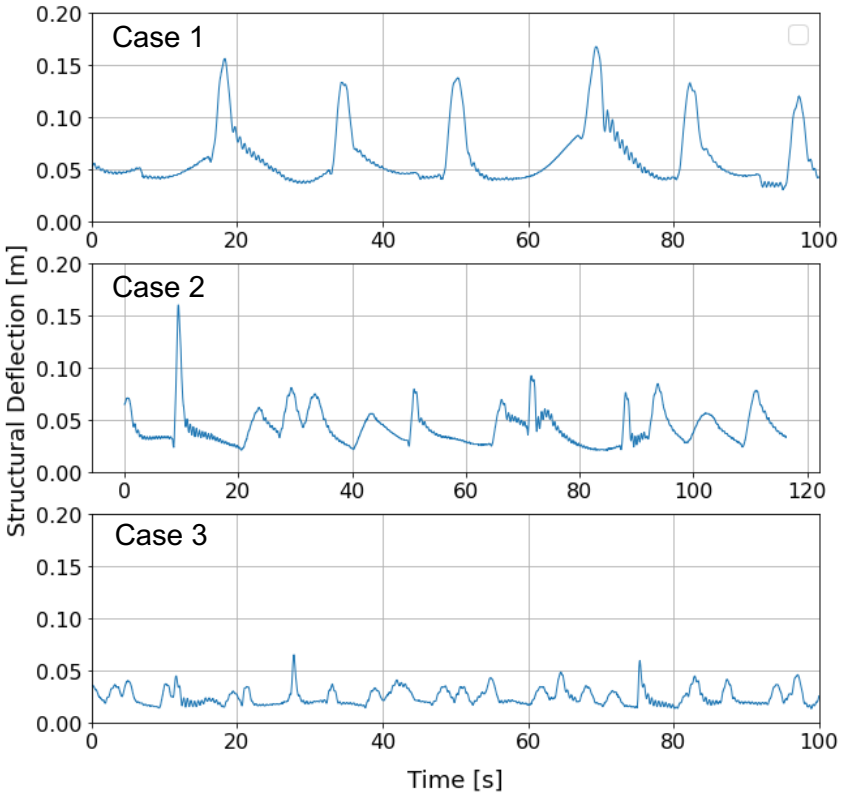

Figure 9 - Computer vision extracted deflection for each test case.

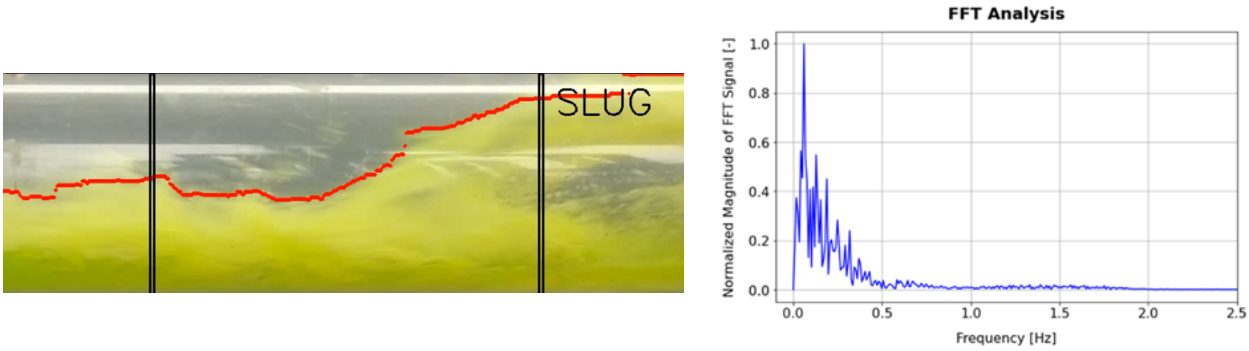

(a) (b)

Figure 10 Example slug identification instance (a) and FFT response frequency analysis (b) for Case 1.

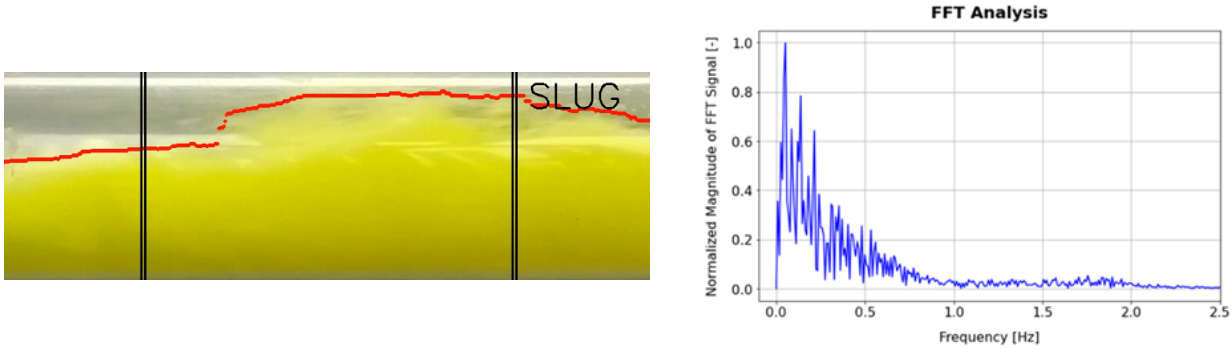

(a) (b)

Figure 11 Example slug identification instance (a) and FFT response frequency analysis (b) for Case 2.

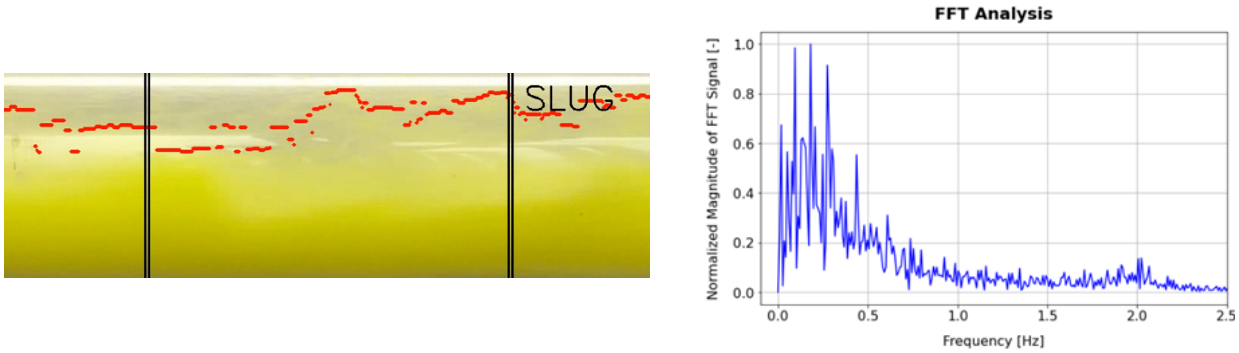

(a) (b)

Figure 12 Example slug identification instance (a) and FFT response frequency analysis (b) for Case 3.

Table 2 presents a summary of the slug characteristics and corresponding average maximum pipe deflection caused by the slugs for all cases investigated in this study. It is observed that as the gas velocity increases, the length of the slug and maximum displacement tend to decrease. In terms of total slug count, an increase in gas velocity leads to a higher number of observed slugs. Furthermore, as previously discussed, the slug frequency

increases with increasing gas velocity. The insights provided in Table 2 are valuable for understanding the overall internal and system response, which is typically utilized in the industry to model slug flow and the loading it creates.

Test Case	Observed Slug Count	Average Slug Length [m]	Average Slug Frequency [Hz]	Pipe Response Frequency [Hz]	Average Max Deflection [m]
Case 1	7	2.19	0.058	0.060	0.14
Case 2	6	1.40	0.050	0.052	0.09
Case 3	27	1.25	0.225	0.180	0.04

Table 2 - Slug characteristics and system response for investigated conditions.

5. CONCLUSIONS

In summary, this paper presents a novel approach that uses computer vision to extract the overall pipe response and complex internal flow (slug) from experimental data. The paper focuses on identifying slug events coupled with the global system structural response and provides numerous benefits for validating numerical and theoretical models. The results of our study demonstrate the effectiveness and usefulness of the approach, highlighting its robustness and scalability to a wide range of complex internal flow patterns.

Furthermore, a detailed analysis of the accuracy of our computer vision methodology revealed good agreement with liquid holdup measurements obtained from conductance probes. Although there were some discrepancies in maximum predicted liquid holdup values, our method demonstrated robustness and scalability compared to the conductance probe signal processing and its limitation to monitor the full system instead of discrete locations. This is a crucial factor in ensuring accurate and reliable results for model validations.

Lastly, we investigated the effects of superficial gas velocity on the system response and observed several key findings. Increasing gas velocity resulted in a decrease in the maximum pipe deflection, indicating a stabilizing effect on the system. We found that increasing the gas velocity resulted in a corresponding increase in the slug frequency, which closely matched the dominant frequency of the pipe response. This suggests that slug frequency is a key factor in governing the system response. Finally, we observed that increasing the gas velocity led to a higher total count of observed slugs, indicating a greater frequency of slug events. These results have important implications for understanding the fluid-structure interaction behavior under varying flow conditions and provide valuable insights for numerical modeling validation.

ACKNOWLEDGEMENTS

The authors recognize the support of TUFFP (Tulsa University Fluid Flow Projects) not only for sponsoring this work but for their outstanding facilities and the technical expertise of their research technicians and flow loop operators. Authors will also want to recognize the partnership between Anaconda Inc. and the McDougall School of Petroleum Engineering Department at the University of Tulsa, which made this collaboration possible.

REFERENCES

Ahmed, W. H. (2011). Experimental investigation of air-oil slug flow using capacitance probes, hot-film anemometer, and image processing. *International Journal of Multiphase Flow, https://doi.org/10.1016/j.ijmultiphaseflow.2011.05.007*, 37(8), 876–887.

Bradski, G. (2000). The OpenCV Library. *Dr. Dobb's Journal of Software Tools*.

Garrido-Jurado, S., Muñoz-Salinas, R., Madrid-Cuevas, F. J., & Marín-Jiménez, M. J. (2014). Automatic generation and detection of highly reliable fiducial markers under occlusion. Pattern Recognition, 47(6). https://doi.org/10.1016/j.patcog.2014.01.005.

Kansao, R., Casanova, E., Blanco, A., Kenyery, F., & Rivero, M. (2008). Fatigue Life Prediction Due to Slug Flow In Extra Long Submarine Gas Pipelines. *https://proceedings.asmedigitalcollection.asme.org.*

Mesa, J. D., Yiannis, C., & Gao, H. (2022). Prediction and benchmarking of a nearly horizontal flowline slug flow. *International Conference on Offshore Mechanics and Arctic Engineering.* Vol. 85925. American Society of Mechanical Engineers.

Miwa, S. M. (2015). Two-phase flow induced vibration in piping systems. (pp. 270-284). . In Progress in Nuclear Energy (Vol. 78). Elsevier Ltd. https://doi.org/10.1016/j.pnucene.2014.10.003.

Mohmmed, A. O., Nasif, M. S., Al-Kayiem, H. H., & Time, R. W. (2016). Measurements of translational slug velocity and slug length using an image processing technique. *Flow Measurement and Instrumentation*, 50, 112–120. https://doi.org/10.1016/j.flowmeasins.

Porter, K., Pereyra, E., Mesa, J., & Sarica, C. (2022). Fluid-Pipe Interaction in Horizontal Gas-Liquid Flow. Proceedings - SPE Annual Technical Conference and Exhibition. OnePetro.